Published in final edited form as:
J Phys Chem B. 2011 January 20; 115(2): 397–405. doi:10.1021/jp108871m.

Conformational analysis of a nitroxide side chain in α-helices with Density Functional Theory

Dora Toledo Warshaviak[†,‡], **Laura Serbulea**[‡], **K. N. Houk**[*,‡], and **Wayne L. Hubbell**[*,†,‡]
[†]Jules Stein Eye Institute, UCLA School of Medicine, Los Angeles, CA 90095
[‡]Department of Chemistry and Biochemistry, University of California, Los Angeles, CA 90095

Abstract

In site directed spin labeling, a nitroxide side chain is introduced at a selected site in a protein; the most commonly used is a disulfide-linked side chain designated R1. The EPR spectra of R1, and the interspin distance between pairs of R1 residues as determined by dipolar EPR spectroscopy, encode a wealth of information on the protein structure and dynamics. However, to extract this information requires structural and dynamical models of the R1 side chain, i.e. the favored rotamers, the intraresidue interactions that stabilize them, and the internal modes of motion. X-ray crystal structures of R1 in proteins have revealed a set of preferred rotamers in the crystal lattice. To identify the intraresidue interactions that stabilize particular rotamers of R1 in the absence of interactions with nearby sidechains in a helix, and to evaluate models for the internal motion of the side chain, quantum mechanical calculations were performed on a relevant fragment of R1 in a ten-residue α-helix. Relative rotamer energies were determined in the gas phase, and solvation energies were estimated from a continuum solvent model that includes both electrostatic and hydrophobic contributions. The results identified preferred rotamers that are in agreement with the X-ray crystallographic studies. The rotamers are apparently stabilized by intra-residue sulfur-backbone interactions, suggesting that the preferred rotamers may be the same at all solvent-exposed helix sites.

Keywords

site-directed spin labeling; nitroxide side chain; quantum mechanics; sulfur-backbone interaction

Introduction

Site directed spin labeling (SDSL) is a powerful technique to study protein structure and dynamics (for reviews see[1–6]). In SDSL, a paramagnetic nitroxide side chain is introduced at a selected site by mutating the native residue to cysteine and then modifying the reactive SH group with a thiosulfonate reagent to produce the disulfide-linked nitroxide side chain designated R1 (Figure 1a). Numerous other nitroxide side chains have been investigated,[7–9] including one introduced *via* a genetically encoded unnatural amino acid,[10] but to date R1 has proven the most useful and is the subject of the present report.

[*]Corresponding authors: K.N. Houk, phone: 310-206-0515, houk@chem.ucla.edu and Wayne L. Hubbell, phone: 310-206-8830, hubbellw@jsei.ucla.edu.

Supporting Information Available: Variation of ΔG_{ele} calculated using Delphi with grid scale and center; Table of X_1 dihedral angles for native and mutant side chains at the same position.
This material is available free of charge via the Internet at http://pubs.acs.org.

The EPR spectrum of R1 in a protein reflects the motion of the nitroxide on a nanosecond time scale. This motion has contributions from Brownian rotational diffusion of the entire protein, R1 internal motions (torsional oscillations about bonds in R1) and local backbone fluctuations on the ps-ns time scale. When necessary (for proteins < 50kDa) the contribution from overall rotational diffusion is effectively removed by employing a viscous solution wherein the EPR spectra reflect only motion of the nitroxide relative to the protein.[11] R1 internal motions can be modulated by interactions of the nitroxide ring with nearby side chains, resulting in sensitivity of the motion to details of the protein tertiary structure.[8,12,13] On the other hand, R1 side chains on the solvent exposed surface of helices, where interactions of the nitroxide ring are absent, present particularly simple situations with single-component EPR spectra ; the motion of the nitroxide has contributions only from R1 internal motions and backbone fluctuations. If one had a quantitative model for R1 internal motion, it would be possible to identify the contribution from backbone flexibility[6,14] which is now recognized to be of importance in protein function.[6,14–18] For this purpose, it is then necessary to seek a model for R1 internal motion.

R1 internal motion is expected to depend on the R1 rotamers and the interactions that stabilize them, and these must be characterized. Progress in identifying the preferred rotamers of R1 has come from X-ray crystal structures of R1 in T4 Lysozyme.[12,13,19,20] It is notable that in all structures to date the set of allowed dihedral angles that define the rotamer is similar for R1 at lattice contact or non-contact sites. For solvent-exposed surface sites well-resolved electron density is only observed for the atom group [C_β---S_γ---S_δ], which allows the determination of only the first two dihedrals, i.e. {X_1, X_2} (see Figure 1a for definitions of the dihedral angles). In the structures solved to date (Table 1), with rare exception, nitroxide side chains adopt one of only 3 rotamers with respect to the {X_1, X_2} dihedrals, namely {m,m}, {t,p} and {t,m}, in that order of popularity (nominally, m = −60, p = +60 and t = 180;[21] this convenient notation is retained for deviations up to ±30° from these nominal values). The two exceptions are located at sterically strained sites.[13,20] Remarkably, in each of the preferred rotamers the S_δ sulfur of the R1 side chain is in close apposition to a backbone atom, suggesting an interaction which would inhibit rotations about X_1–X_3 and give rise to an internal motion dominated by oscillations about X_4 and X_5 (Fig. 1b). This X_4/X_5 model is supported by EPR spectral lineshape analysis and variation of side chain structure.[6,7,9,22]

Brownian[23–25] and molecular dynamics[26–28] have been applied to describe the internal motion of R1. With suitably accurate force fields, sufficiently long trajectories and proper sampling of conformational space these approaches should in principle provide a detailed picture of R1 internal modes. But, so far the results do not reveal the unique stability of the rotamers observed experimentally despite recent improvements in conformational sampling[29,30] and parametrization[31] of the spin labels. Quantum mechanical (QM) methods, despite being computationally expensive, do not rely on empirical parameters and often result in more accurate determination of molecular conformations and relative energies. Such an approach was used recently for conformational analysis of the R1 side chain[32]. In that study, ab initio calculations of the torsional profiles of fragments of R1 were performed at the HF/6-31G** level. These calculations revealed 18 possible conformations for R1 side chain and their probabilities. The {m,m} rotamer was found to be most probable, in agreement with experimental results, but a low probability was assigned to the commonly observed {t,p} state; the experimentally observed {t,m} state was not included among the possible rotamers. Moreover, the {m,t} rotamer, experimentally observed at only a single sterically hindered site, was given a high probability of occurrence. The discrepancies between experimental and theoretical results is in part due to the fact that the energy profiles for dihedral angles other than X_1 were calculated using fragments of the R1 side chain without backbone atoms. As a result, the experimentally observed interaction between S_δ

and backbone atoms was not included as a possibility and the consequences of the interaction were ignored.

The Hartree-Fock (HF) theory employed by Tombolato *et al.*[32] might not be the most suitable method to explore interactions of R1 with the backbone due to its neglect of electron correlation, which is important for correct representation of interactions of the sulfur atoms with the backbone atoms. The importance of including electron correlation in describing weak hydrogen bonds and the interaction between chalcogen centers (O, S, Se, Te) has been discussed previously.[33,34] In the study reported here, Density functional Theory (DFT), which includes electron correlation effects with reasonable computational cost, was employed to compute the relative gas phase energies of rotamers for an R1 fragment in a single amino acid and in a ten residue α-helix. Comparisons of energies of conformational minima were computed with dispersion energy corrections (DFT-D), to account for stabilizing nonbonding interactions that occur in some conformations. Solvation energies, both electrostatic and non polar, were estimated from a continuum solvent model, and the total energies revealed preferred rotamers that were generally in good agreement with those observed in crystal structures. As anticipated, a major determinant of the stability of these rotamers is the backbone sulfur interaction that has contributions from both non-bonded interactions and solvation effects.

The Computational Model

The focus of this study is on interactions of the sulfur atoms with the peptide backbone and their role in stabilizing particular rotamers. For this purpose, the presence of the nitroxide ring is not essential and was replaced by a methyl group; this side chain will be referred to as R1′, shown modeled in a peptide fragment in Figure 1c. Thus, situations where direct interactions of the nitroxide ring occur with local side chains or backbone atoms are intentionally excluded. As mentioned above, the case of interest here is the solvent-exposed non-interacting site.

Geometries and relative conformational energies ($\Delta(E+D)_{conf}$) of allowed R1′ rotamers were first obtained in the gas phase from DFT. The R1′ gas phase conformations from DFT are then employed to compute both the electrostatic (ΔG_{ele}) and non-polar (ΔG_{np}) contributions to the relative solvation free energies using a continuum solvent model. The total relative free energies are then computed as $\Delta G_{tot} = \Delta(E+D)_{conf} + \Delta G_{ele} + \Delta G_{np}$. The addition of the relative electronic conformational energy to free energies of solvation to obtain a total free energy is justified under the assumption that the differences in conformational entropies between rotamers are small. This assumption is reasonable for the small side chain considered here and defines a feature of the model to be evaluated by comparison of the results with experiment. The paragraphs below outline the calculation for each term.

Quantum Mechanical Conformational Energies in the gas phase

DFT computations were performed at the B3LYP/6-31G(d) level using the Gaussian 03 package[35] to optimize molecular geometries. The energies of the various minima were recalculated with a dispersion energy correction (B3LYP-D),[36] which greatly improves predictions for the relative conformational energies of a polypeptide model.[37] In all calculations backbone φ, ψ and ω angles were fixed at values corresponding to a regular α-helix, −60°, −40° and 180° respectively. Partial atomic charges were determined using the CHelpG algorithm implemented in the Gaussian 03 package with B3LYP/6-31G(d). Details of the procedure are given below in RESULTS.

Solvation Free Energy

Solvation effects can be treated explicitly or implicitly. Describing the solvent effect explicitly in atomic level by calculating actual solvent-solute interactions is not feasible in quantum mechanical calculations. An alternative approach taken here employs an implicit model in which the solvent is represented as a continuum dielectric, and empirical terms are used for the interaction of surface atoms with solvent (ΔG_{np}). In the context of this model, the solvation free energy (ΔG_{sol}) for transferring a molecule from the gas phase to water can be written as

$$\Delta G_{sol}=\Delta G_{np}+\Delta G_{ele} \quad (1)$$

where ΔG_{np} is the free energy for transferring an uncharged analogue of the molecule into water from the gas phase, and ΔG_{ele} is the electrostatic contribution due to charges in the protein (ε=2) interacting with a continuum of dielectric constant ε =80.[38] ΔG_{np} is taken to be proportional to total solvent accessible surface area[39] of a molecule according to

$$AG_{np}=\gamma_{vw}A_T \quad (2)$$

where γ_{vw} is the vacuum-to-water surface tension coefficient. This value lies in the range of 25 –50 cal/mol/A[240–42] and the consequence of variation on the final results will be discussed below. The total solvent accessible surface area A_T is calculated with the program SURFCV[43] using PARSE van der Waals radii[44] and a probe radius of 1.4 Å.

ΔG_{ele} is the difference in electrostatic free energy of a molecule in water (ε =80) and the gas phase (ε =1), and is computed as described by Sitkoff *et al.*[44] from the finite difference Poisson–Boltzmann method implemented in the program Delphi[45]. Thus,

$$\Delta G_{ele}=\frac{1}{2}\sum q_i(\Phi_i^{80}-\Phi_i^{1}) \quad 3$$

where q_i is a point charge at the i^{th} grid point, Φ_i^{80} is the corresponding electrostatic potential calculated with solvent dielectric constant 80 and solute (protein) dielectric constant 2[46] and Φ_i^{1} is the electrostatic potential calculated with solvent dielectric constant 1 and solute dielectric constant 2.

The continuum approach has been shown to have comparable accuracy to explicit models in calculation of total solvation free energies.[38,46,47] It has been used extensively in combination with molecular mechanics to determine solution conformations of molecules[48–52] and also in combination with ab initio quantum mechanics to determine solvation free energies of organic molecules[53].

Calculations of ΔG_{np} and ΔG_{ele} were performed in DELPHI using gas phase optimized structures from QM. Charges and atomic radii were taken from the PARSE set,[44] optimized for calculation of solvation energies. The geometric center of a molecule was placed in the center of a cubic grid with a resolution of 2.8 grids/Å. The grid size was adjusted so that only 80% of the grid was filled with the molecule, which corresponded to 55–63 grids per side for different conformations. The water probe radius was 1.4 Å and Coulombic boundary conditions were used. A convergence criterion was set to 10^{-4} k_BT where k_B is the Boltzmann constant and T is the absolute temperature. The grid scale (from 2.0–3.0 grids/Å in 0.2 grids/Å increments) and center were varied for three different conformations in order to check the accuracy of the calculations. ΔG_{ele} values varied with grid scales in the range

2.0–2.4 grids/Å, but differed by less than 0.1 kcal/mol in the range 2.6–3.0 grids/Å; 2.8 grids/Å was employed in all calculations. The grid offset was varied ±0.5 grid units in 0.1 increments for three conformations for a grid scale of 2.8 grids/Å and 2.0 grids/Å. The position of the molecules on the grid affected ΔG_{ele} for a grid scale of 2.0 grids/Å but caused a change of less than 0.2 kcal/mol for a scale of 2.8 grids/Å (see Figure S1, Supporting Information).

Results

QM calculations for R1′ in a model peptide unit (Figure 1c) were first performed to determine the minima for X_1 and X_2 angles. Conformations corresponding to the energy minima were then built in the center of a ten residue polyglycine α-helix (Figure 2) and optimized to find the most probable R1′ conformations in a helical environment.

X_1, X_2 energy minima of R1′ in a model peptide unit

A scan of X_1 for R1′ in the model peptide unit of Figure 1c was carried out. During the scan X_2 was set to the known minima for tetrahedral carbon atoms, (−60, 180 or +60) and X_3 was set to the disulfide torsional minima (±90). X_1 minima classified as {m}, {p} and {t} were found (Figure 3) independent of X_2 and X_3 angles, in agreement with results from an earlier HF calculation.[32] Among these minima, the {m} conformation was the lowest energy conformation. The {p} conformation of X_1 cannot exist at α-helical sites due to steric clashes of Sγ with the helical backbone, also observed previously.[32] Hence, for a α-helical site, X_1 of the R1 side chain can only be in the {m} or {t} conformation, {m} being the lowest energy (most probable).

Unlike the case for the X_1 torsional potential profile, that for X_2 depends on the values of the other dihedrals (Figure 4a and 4b). When X_1 was {t}, three energy minima were observed for X_2 at {m}, {p} and {t}, with {p} being the lowest (Figure 4a). When X_1 was {m} three minima were again observed for X_2 but of rather similar energy (Figure 4b). In the calculations of Tombolato *et al.* the X_2 potential profile was computed for a fragment without backbone atoms and the X_1 dependence on the X_2 energy profile was not noted[32].

Gas phase energy minima of R1′ in a ten residue α-helix

With two possible minima for X_1 and three minima for X_2 observed from the torsional scans in a single residue peptide segment, six possible low energy conformations were considered for the R1′ side chain with respect to these dihedrals: {m,m}, {m,p}, {m,t}, {t,m}, {t,p}, {t,t}. Molecular modeling of these conformations in a helix showed steric clashes of S_δ and C_ε atoms with the backbone for {m,p} eliminating the possibility of this rotamer at helical sites. In order to identify new interactions and to determine the relative energies of the remaining five {X_1, X_2} conformations in a helical environment, each was built using R1′ situated in the middle of a ten residue α-helix (Figure 2). For each conformation the X_3 angle was set either to +90° (p) or −90° (m)[54] generating 10 possible {X_1, X_2, X_3} combinations for R1′. For each of the 10 starting conformers, the energy was minimized keeping the structure of the helix fixed. Selected interatomic distances, torsion angles and relative gas phase energies are given for the optimized conformations in Table 2. Figure 5 shows models of the optimized conformations; only 9 conformations are identified in the Table 2 and Figure 5 because the {m,t,m} starting configuration relaxed to {m,m,m} during optimization (see below).

Interactions that stabilize the rotamers in a helical environment

To identify interactions that stabilize one rotamer of R1′ relative to another, it is assumed that an interatomic distance at or near the sum of the van der Waals radii for two atoms

implies an attractive interaction relative to another rotamer where the atoms are separated. For X_1, the energy minima for the allowed {m} and {t} states of R1′ (Figure 3) occur when S_γ lies within attractive interaction range of the backbone N and O, respectively. This is the case for any side chain with an atom at the γ position, and these interactions presumably contribute to the stability of the {m} and {t} states. Indeed, when a native side chain is mutated, the new side chain maintains a X_1 state close to that of the native residue (see Table S1, Supporting Information), indicating that interactions with the backbone are more important than details of the side chain structure.

For a given value of X_1, the values of X_2 and X_3 in R1′ determine the positions of the S_δ atom and the $C_\varepsilon H_3$ groups, respectively, relative to backbone atoms, and consequently their interactions. These interactions are easily appreciated in the models of Figure 5 which are intended to accompany the following description. In the four lowest energy states, the {X_1, X_2} combinations, namely {m,m}, {m,t} and {t,p}, all place the S_δ atom within interaction distance of $C_\alpha H$, suggesting a $C_\alpha H\cdots S_\delta$ attractive interaction that stabilizes these states. For {m,m} and {t,p}, this interaction is intra-residue; for {m,t} the interaction is inter-residue, involving the $C_{\alpha(i-3)}H$, and unique to the helix geometry. To establish this interaction, X_2 is distorted by nearly 30° from the nominal *trans* value (Table 2). The initial {m,t,m} configuration was unstable due to C_ε being very close to $C_{\alpha(i-3)}$ and relaxed to {m,m,m} after optimization; thus only a single {m,t} rotamer is allowed. As shown below, the {m,t} state is strongly destabilized by solvation.

In the {t,m} states the S_δ atom also makes an apparent stabilizing interaction with the backbone, but in this case with the O atom of the backbone C=O. For both states, the interatomic distance of $S_\delta\cdots O$ is greater than the sum of the van der Waals radii. Note also the unusually large absolute value of X_2 in the {t,m} rotamers, nearly 30° from the nominal {m} value. In the higher energy {t,t} states, the {t} configuration of X_2 moves the S_δ atom away from the backbone and attractive interaction with both C=O and $C_\alpha H$ are lost; only $S_\gamma\cdots O{=}C$ interactions stabilize the rotamer conformations.

The value of X_3 modulates the energy of the {X_1, X_2} states *via* positioning of the $C_\varepsilon H_3$ for attractive or repulsive steric interactions. For example, the {t,p,p} state is higher in energy than {t,p,m} due to loss of an attractive interaction of the $C_\varepsilon H_3$ group with the Oxygen of the backbone C=O; {t,m,m} is of higher energy than {t,m,p} due to loss of the same interaction; {m,m,p} is of higher energy than {m,m,m} due to repulsive interactions of the methyl group with backbone atoms. These interactions involving the $C_\varepsilon H_3$ are shown in the models of Figure 5, and offer qualitative explanations for the energy differences between rotamers in the gas phase.

Evidence for the $C_\varepsilon H_3\cdots O{=}C$ interaction in {t, p, m} and {t, m, p}, other than the close proximity of the atoms (d($C_\varepsilon H\cdots O{=}C$=2.35 Å in {t,p,m} and d($C_\varepsilon H\cdots O{=}C$=2.21 Å in {t,m,p}), comes from the increase in charge (determined from QM) on the C_ε atom when in proximity to O=C in each case.[55] For {t, p, p} and {t, m, m}, where the groups are separated, the charge is −0.15 and −0.23, respectively. In the putative interacting configuration, the charge is +0.03 and −0.01, respectively. In addition, there are slight differences in conformation of R1′ required to accommodate the interaction such as larger $S_\delta\cdots O{=}C$ distance in {t, p, m} and {t, m, p} compared to {t, p, p} and {t, m, m}, respectively (Table 2).

Effect of solvation

The quantum mechanical calculations presented above were carried out for the system in a vacuum. The effects of an aqueous solvent on the relative conformational energies include contributions from screening of pairwise Coulombic interactions and from electrostatic and

non-polar contributions to the solvation energy that can be estimated from the continuum solvent model as described above.

The relative gas phase conformational free energy from DFT, the individual contributions to the solvation free energy, and the total free energy of the R1′ rotamers in the helix are reported in Table 3, listed in order of increasing total energy. A major effect of solvation is to raise the energy of the {m,t} state relative to the others. The origin of this effect will be discussed below. As in the gas phase, the {t,t} state has the highest energy.

Discussion

According to arguments presented in the introduction, knowledge of the stable rotamers of R1 and the interactions responsible for their stability is important for employing the side chain to monitor backbone dynamics in proteins. In addition, such information can improve the interpretation of inter-spin distance measurements between R1 residues in terms of protein structure.[56,57] To this end, both experimental and theoretical approaches are being taken. On the experimental side, 9 crystal structures of R1 in T4 Lysozyme have been reported that define a clear set of stable rotamers with respect to $\{X_1,X_2\}$ (Table 1). Even though many of these sites were not at crystal lattice contacts, and some structures were determined at ambient as well as cryogenic temperatures, concern has been raised that the crystal lattice conditions may play a role in selecting rotamers, and that different rotamers with different stabilizing interactions may exist in solution. This sentiment is partly based on Molecular Dynamic simulations of R1[31] that predicted a different set of populated rotamers at 131R1 in T4L than observed in the crystal structure.[19]

The goal of the present work was to determine whether or not an appropriate QM treatment would predict a set of most stable rotamers in agreement with those seen in crystal structures and identify the stabilizing interactions. The results presented here for R1′ improve and extend an earlier HF calculation[32] in several ways. First, the present work uses DFT which accounts for electron correlation effects important in treating interactions involving sulfur and weak hydrogen bonds.[33,34] Second, R1′ was investigated in a single peptide unit or a polyglycine helical structure rather than as an isolated fragment; one of the major conclusions from the current study is that intra-residue and longer range interactions in a helical structure are important in stabilizing particular rotamers. Finally, solvation effects were investigated using a continuum solvation model employing PARSE parameters developed specifically for the Finite-Difference Poisson Boltzmann / γ_{vw} (FDPB/γ) model (44) that was used here. This model reproduced experimental solvation energies with a mean deviation of 0.44 kCal/mole for 67 small molecules, including polar molecules capable of H-bonding, and 0.16 kCal/mole for amino acid side chains and peptide backbone analogs (44). While there are uncertainties in any solvation model, and an unknown magnitude of effects for particular cases, including the present one, it is felt that the approach taken here is a valid one, particularly considering the respectable agreement with experiment. The key results of this study and how they relate to the conformations observed in X-ray crystal structures of R1 attached to T4 Lysozyme are discussed below.

R1′ conformational energies from DFT and the effects of solvation

Based on the relative energies computed from DFT, the five most stable rotamers of R1′ in an α-helix in the gas phase are {t,p,m}, {m,m,p}, {t,m,p}, {m,m,m} and {t,m,m} (Table 3). Notably, all represent the three favored $\{X_1, X_2\}$ rotamers observed in the crystal structures, namely {m,m}, {t,p} and {t,m}; the {t,t} rotamers, not yet observed in any crystal structure, have the highest relative energies.

As illustrated in Figure 5, the favored rotamers are apparently stabilized by intra-residue Sulfur-backbone interactions and, in the case of {t,m} and {t,p}, by additional $C_\varepsilon H$-backbone interactions. The interatomic distances that reveal these interactions, as determined from DFT (Table 2), deviate no more than 0.36Å from those determined from crystal structures of R1 (Table 1). For example, the experimental values for the $C_\alpha H\cdots S_\delta$ distance lie in the range 2.65 – 3.07 Å for the {m,m} rotamer, while the calculated values are 3.01 and 3.17 Å for the two {m,m} states. Likewise, for the {t,p} states, stabilized by the same interaction, the experimental values lie in the range 3.12 – 3.26 Å; the corresponding calculated distances are 3.04 and 3.11 Å. Finally, for the less stable {t,m} states stabilized by $S_{\gamma,\delta}\cdots O{=}C$ interactions, experimental values are in the range 3.29 – 3.73 Å, while DFT gives 3.82 Å. For {t,m}, the relatively large $S_\delta\cdots O$ distance corresponds to the large $|X_2|$, which is ≈ 30° greater than the nominal value of an {m} state.

The {m,t,p} rotamer is predicted to be of low relative energy by DFT in the gas phase, but is strongly disfavored by solvation. It should be noted that the relative solvation energies in Table 3 did not change significantly when γ_{vw} values of 25 kcal/mol were used instead of 50 kcal/mol;[40–42] the non-polar term is relatively small in general. They also did not depend on the charged set used (PARSE vs. CHelpG) for the calculations performed in the 10 residue helix. The following qualitative account of solvation interactions sheds some light on the solvent destabilization of the {m,t,p} rotamer. .

The purely electrostatic contribution to the free energy of solvation, ΔG_{ele}, is always negative (favorable) because charges on the protein interact favorably with a high dielectric solvent (water). The magnitude depends strongly on details of protein surface topography; as a consequence neighboring residues in a helix can have a strong effect on ΔG_{ele}. In general, for two rotamers of R1′, the one with the largest surface exposed to solvent will have the most favorable ΔG_{ele}.

The purely non-electrical contribution to solvation, ΔG_{np}, is basically the hydrophobic effect and is always positive (unfavorable); its magnitude is proportional to the solvent exposed surface area and the surface tension coefficient γ_{vw}. For two rotamers of R1′, the one with the largest exposed surface area will have the most unfavorable ΔG_{np}. Thus, the two contributions to solvation act in the opposite direction and cancel each other to some extent, although the ΔG_{ele} term can be much larger than ΔG_{np} for R1′ (Table 3).

As anticipated from the above considerations, the data in Table 3 shows that rotamers with low conformational free energies have high ΔG_{ele} contributions and *vice versa;* the correlation arises simply because the most strongly interacting states are well packed and are hence most desolvated. The {m,t,p} state in the helix has one of the lowest conformational energies, due to the inter-residue $C_{\alpha(i-3)}H\cdots S_\delta$ and other interactions, and is thus strongly destabilized by the ΔG_{ele} contribution which dominates the overall energy; details of the charge distribution and local topography contribute to the unusually unfavorable solvation term.

Another interesting effect of solvation is noted for the favored {t,p} states. In particular, the {t,p,p} state, in which the $-C_\varepsilon H_3$ group projects away from the backbone, is inherently much less stable in the gas phase than {t,p,m} ($\Delta\Delta G_{conf} \approx 4.2$kcal/mol) where the $-C_\varepsilon H_3$ group makes a stabilizing interaction with the Oxygen of the backbone (Figure 5c). However, in energy gap between the two states is reduced to ≈ 2 kcal/mole due to a strongly stabilizing contribution of ΔG_{ele} to the more solvent exposed {t,p,p} state.

The magnitude of the total energy differences between rotamers in the solvated helix is small, with a range of ≈ 3.4 kcal/mole; at ambient temperature, this corresponds to a preference of >99% for the rotamer of lower energy. However, given the simple model

employed here, not much significance should be attached to the absolute differences in energy. Perhaps the most important conclusion is the rotamers of the {m,m}, {t,p} and {t,m} class are grouped at lower energies than those of the {t,t} or {m,t} class. Members of the lower energy group have attractive intra-residue interactions between S_δ and backbone atoms, either $C_\alpha H\cdots S_\delta$ ({m,m}, {t,p}) or $S_\delta\cdots$-O=C {t,m}, the same interactions postulated based on crystal structures.; these interactions are absent in {t,t} and {m,t}.

The chemical nature of the stabilizing interactions

The rather nonconventional S···X (X=C,O,N) interactions of sulfur with the backbone atoms have been previously demonstrated to contribute significantly to protein stabilization in theoretical and experimental studies[12,13,19,20,33,58–62]. The Sulfur atom acts either as a weak hydrogen bond acceptor in X-H···S interactions or is involved in S···X nonbonded interactions, both of which have directional preferences of the X with respect to S.[33,59–62]

In the nonbonded interaction characterized by p(X)-σ*(S) orbital overlap, the electron-rich nucleophile (O or N) tends to approach S along the S-S or C-S bond and within 30° of the S-S-C plane.[61–64] In the putative $C{=}O\cdots S_\gamma$-S_δ (in {t,t,m}) and $C{=}O\cdots S_\delta$-C_ε (in {t,p,p}, {t,m,m}) interactions, the oxygen atom does not lie along the extension of C-S or S-S bond, which prevents optimal p–σ* orbital overlap, weakening this interaction. In addition, the S···O distance observed in {t,p,p}, {t,m,m} and {t,t,m} is larger than the sum of corresponding van der Waals radii (r_{vdW}(S···O)=3.32 $Å_{65}$) further suggesting a weak interaction. However, the average S···O distance in putative attractive interactions involving sulfur and main chain carbonyl oxygen atoms was reported to be 3.6 Å in a study of 572 disulfide bonds in 247 polypeptide chain from the Protein Data Bank[58], similar to the values observed here (Table 2). Also, quantum mechanical calculations indicated an intermolecular distance of 3.46 Å between sulfur and oxygen in organic compounds when oxygen and sulfur were the electron donating and accepting units, respectively.[59]

The putative N···Sγ (in {m,m},{m,t}) and $C\cdots S_\delta$ (in {mm},{tp}) interactions can in principle involve both X···S and X-H···S (X: N, C) attractive interactions.[61,66] The $CH\cdots S_\delta$ interaction was previously suggested to be a nonclassical hydrogen bond.[20] In R1′ conformations stabilized by $CH\cdots S_\delta$ interactions, the, $CH\cdots S_\delta$ distance (3.54 – 3.65 Å) and the $\angle_{C\text{-}H\text{-}S}$ (107–110°) determined both from the quantum mechanical model presented here ($CH\cdots S_\delta$ distance in the range 3.54 – 3.65 Å and $\angle_{C\text{-}H\text{-}S}$ in the range 107–110°) and experimental studies[19] deviates slightly from the characteristic angle $\angle_{C\text{-}H\text{-}S} \geq 120°$ and $CH\cdots S_\delta$ distance ≤3.5 Å[67], suggesting a weaker contribution of the hydrogen bonding interaction to stability of {m,m} and {t,p} rotamers based on this criterion. Nevertheless, the short $C\text{-}H\cdots S_\delta$ distance, in some cases less than the sum of the H and S van der Waals radii,[19] indicates a possible H bonding interaction. A “1,4 interaction” between sulfur and CH group that is less directional than the C-H···S hydrogen bonds discussed by Weiss *et al.*[67] but comparable to it in strength (1–2 kcal/mol) were previously reported.[66,68]

In R1’ conformations stabilized by possible $NH\cdots S_\gamma$ interactions, the $NH\cdots S_\gamma$ distance and the $\angle_{N\text{-}H\text{-}S}$ angle are in the range of favorable hydrogen bonding interaction (d≤3.5 Å, $\angle_{N\text{-}H\text{-}S} \geq 90°$).[67] In addition, these conformations could be stabilized by p(N)-σ*(SS)[61] interaction, but the nitrogen atom does not lie along the extension of the S-S bond which prevents optimal p–σ* orbital overlap.

The C_ε-H···O=C interaction may be another weak hydrogen bonding in the {t,p,m} and {t,m,p} conformations. This type of interaction has been previously reported[59,61,67,69]. Ab initio calculations at the MP2/6-31G(d) level of model complexes (CH_3SSCH_3 + $CH_3CONHCH_3$ and CH_3SCH_3 + $CH_3CONHCH_3$) having S···X (X=C,O,N) interactions revealed stabilization energies of 3.2 kcal/mol for S-S···O and of 2.5 kcal/mol for C-S···O,

including the contribution from a C=O···H-C interaction that is also present in those complexes.[61] The p–σ* orbital interaction was estimated to be 0.64 kcal/mol[61] which suggests significant contribution of a hydrogen bond to complex stability. This has also been suggested for model oxygen containing complexes in which weak hydrogen bonding between methyl group and oxygen atom is stronger than the interaction between sulfur and oxygen.[59] The lower energy of {t,p,m} compared to {t,p,p} and {t,m,p} compared to {t,m,m} is due to the greater contribution of C=O···H-C relative to S···O interaction to stability of {t,p,m} and {t,m,p} (Figure 5).

In summary, R1′ is mainly stabilized by the interaction of the sulfur groups with the backbone atoms (C_α-H, N-H and C=O groups) and by C_ε-H···O=C interaction. Among these C_α-H···S_δ. and N-H···S_γ are likely to be the most important interactions. Both weak hydrogen bonding is involved in these interactions in addition to 1,4 carbon-sulfur interaction in C_α-H···S_δ..and p-σ* interaction in N-H···Sγ.

Conclusion

Based on a very simple model that takes into account the influence of solvent, it is found that the most stable group of rotamers of the R1′ disulfide-linked side chain in a polyglycine helix corresponds to that observed in crystal structures with regard to the first two dihedral angles (X_1, X_2). Although interactions with nearby side chains in a native helix will influence relative rotamer energies, the results presented here are expected to apply to R1 at solvent exposed non-interacting sites. Such sites are readily recognized in the EPR spectrum, and are in fact the most interesting for extracting the contribution to motion of the nitroxide from backbone flexibility.[6,14] The members of the group of favored rotamers are apparently stabilized by Sulfur-backbone interactions. The fact that the stabilizing interactions that determine {X_1, X_2} are essentially all intra-residue suggests that the preferred {X_1, X_2} rotamers will be the same at all solvent-exposed helix sites, independent of sequence and probably not strongly dependent on details of the local backbone dihedral angles.

Supplementary Material

Refer to Web version on PubMed Central for supplementary material.

Acknowledgments

This research was supported by National Institute of Health grants GM- 075962 to KNH and EY-05216 to WLH and the Jules Stein Professorship endowment to WLH. The authors thank Steven E. Wheeler (Texas A&M) for the dispersion correction calculations, Mark R. Fleissner for reading the manuscript thoroughly.

References

1. Hubbell WL, Cafiso DS, Altenbach C. Nat Struct Mol Biol. 2000; 7:735.
2. Hubbell WL, Gross A, Langen R, Lietzow MA. Current Opinion in Structural Biology. 1998; 8:649. [PubMed: 9818271]
3. Hubbell WL, Mchaourab HS, Altenbach C, Lietzow MA. Structure. 1996; 4:779. [PubMed: 8805569]
4. Fanucci GE, Cafiso DS. Current Opinion in Structural Biology. 2006; 16:644. [PubMed: 16949813]
5. Klug, CS.; Feix, JB. Methods in Cell Biology. Vol. Vol. Volume 84. Academic Press; 2008. Methods and Applications of Site-Directed Spin Labeling EPR Spectroscopy; p. 617
6. Columbus L, Hubbell WL. Trends in Biochemical Sciences. 2002; 27:288. [PubMed: 12069788]
7. Columbus L, Kalai T, Jeko J, Hideg K, Hubbell WL. Biochemistry. 2001; 40:3828. [PubMed: 11300763]

8. Mchaourab HS, Lietzow MA, Hideg K, Hubbell WL. Biochemistry. 1996; 35:7692. [PubMed: 8672470]
9. Mchaourab HS, Kalai T, Hideg K, Hubbell WL. Biochemistry. 1999; 38:2947. [PubMed: 10074347]
10. Fleissner MR, Brustad EM, Kalai T, Altenbach C, Cascio D, Peters FB, Hideg K, Parker S, Schultz PG, Hubbell WL. Proceedings of the National Academy of Sciences. 2009; 106:21637.
11. López CJ, Fleissner MR, Guo Z, Kusnetzow AK, Hubbell WL. Protein Science. 2009; 18:1637. [PubMed: 19585559]
12. Guo Z, Cascio D, Hideg K, Hubbell WL. Protein Sci. 2008; 17:228. [PubMed: 18096642]
13. Guo Z, Cascio D, Hideg K, Kalai T, Hubbell WL. Protein Sci. 2007; 16:1069. [PubMed: 17473014]
14. Columbus L, Hubbell WL. Biochemistry. 2004; 43:7273. [PubMed: 15182173]
15. Schnell JR, Dyson HJ, Wright PE. Annual Review of Biophysics and Biomolecular Structure. 2004; 33:119.
16. Hammes-Schiffer S, Benkovic SJ. Annual Review of Biochemistry. 2006; 75:519.
17. McElheny D, Schnell JR, Lansing JC, Dyson HJ, Wright PE, Petsko GA. Proceedings of the National Academy of Sciences of the United States of America. 2005; 102:5032. [PubMed: 15795383]
18. Boehr DD, Nussinov R, Wright PE. Nat Chem Biol. 2009; 5:789. [PubMed: 19841628]
19. Fleissner MR, Cascio D, Hubbell WL. Protein Science. 2009; 18:893. [PubMed: 19384990]
20. Langen R, Oh KJ, Cascio D, Hubbell WL. Biochemistry. 2000; 39:8396. [PubMed: 10913245]
21. Lovell SC, Word JM, Richardson JS, Richardson DC. Proteins: Structure, Function, and Bioinformatics. 2000; 40:389.
22. Barnes JP, Liang Z, McHaourab HS, Freed JH, Hubbell WL. Biophysical Journal. 1999; 76:3298. [PubMed: 10354455]
23. Steinhoff HJ, Müller M, Beier C, Pfeiffer M. Journal of Molecular Liquids. 2000; 84:17.
24. Robinson BH, Slutsky LJ, Auteri FP. The Journal of Chemical Physics. 1992; 96:2609.
25. Steinhoff HJ, Hubbell WL. Biophys. J. 1996; 71:2201. [PubMed: 8889196]
26. LaConte LEW, Voelz V, Nelson W, Enz M, Thomas DD. Biophys. J. 2002; 83:1854. [PubMed: 12324407]
27. Hakansson P, Westlund PO, Lindahlb E, Edholmb O. Phys Chem Chem Phys. 2001; 3:5311.
28. Timofeev VP, Nikolsky DO. J Biomol Struct Dyn. 2003; 21:367. [PubMed: 14616032]
29. Fajer MI, Li H, Yang W, Fajer PG. Journal of the American Chemical Society. 2007; 129:13840. [PubMed: 17948993]
30. Li H, Fajer M, Yang W. The Journal of Chemical Physics. 2007; 126 024106.
31. Sezer D, Freed JH, Roux B. J. Phys. Chem. B. 2008; 112:5755. [PubMed: 18412413]
32. Tombolato F, Ferrarini A, Freed JH. J. Phys. Chem. B. 2006; 110:26248. [PubMed: 17181283]
33. Bleiholder C, Werz DB, Koppel H, Gleiter R. J. Am. Chem. Soc. 2006; 128:2666. [PubMed: 16492053]
34. Chandra AK, Nguyen MT. Chemical Physics. 1998; 232:299.
35. Frisch, MJ.; Trucks, GW.; Schlegel, HB.; Scuseria, GE.; Robb, MA.; Cheeseman, JR.; Montgomery, JA., Jr; Vreven, T.; Kudin, KN.; Burant, JC.; Millam, JM.; Iyengar, SS.; Tomasi, J.; Barone, V.; Mennucci, B.; Cossi, M.; Scalmani, G.; Rega, N.; Petersson, GA.; Nakatsuji, H.; Hada, M.; Ehara, M.; Toyota, K.; Fukuda, R.; Hasegawa, J.; Ishida, M.; Nakajima, T.; Honda, Y.; Kitao, O.; Nakai, H.; Klene, M.; Li, X.; Knox, JE.; Hratchian, HP.; Cross, JB.; Bakken, V.; Adamo, C.; Jaramillo, J.; Gomperts, R.; Stratmann, RE.; Yazyev, O.; Austin, AJ.; Cammi, R.; Pomelli, C.; Ochterski, JW.; Ayala, PY.; Morokuma, K.; Voth, GA.; Salvador, P.; Dannenberg, JJ.; Zakrzewski, VG.; Dapprich, S.; Daniels, AD.; Strain, MC.; Farkas, O.; Malick, DK.; Rabuck, AD.; Raghavachari, K.; Foresman, JB.; Ortiz, JV.; Cui, Q.; Baboul, AG.; Clifford, S.; Cioslowski, J.; Stefanov, BB.; Liu, G.; Liashenko, A.; Piskorz, P.; Komaromi, I.; Martin, RL.; Fox, DJ.; Keith, T.; Al-Laham, MA.; Peng, CY.; Nanayakkara, A.; Challacombe, M.; Gill, PMW.; Johnson, B.; Chen, W.; Wong, MW.; Gonzalez, C.; Pople, JA. Gaussian 03. Wallingford CT: Gaussian, Inc.; 2004.

36. Grimme S. Journal of Computational Chemistry. 2006; 27:1787. [PubMed: 16955487]
37. Schwabe T, Grimme S. Physical Chemistry Chemical Physics. 2007; 9:3397. [PubMed: 17664963]
38. Honig B, Nicholls A. Science. 1995; 268:1144. [PubMed: 7761829]
39. Lee B, Richards FM. Journal of Molecular Biology. 1971; 55:379. [PubMed: 5551392]
40. Eriksson AE, Baase WA, Zhang XJ, Heinz DW, Blaber M, Baldwin EP, Matthews BW. Science. 1992; 255:178. [PubMed: 1553543]
41. Lee B. Protein Science. 1993; 2:733. [PubMed: 8495196]
42. Serrano L, Sancho J, Hirshberg M, Fersht AR. Journal of Molecular Biology. 1992; 227:544. [PubMed: 1404368]
43. Sridharan S, Nicholls A, Honig B. Biophys. J. 1992; 61:A174.
44. Sitkoff D, Sharp KA, Honig B. J. Phys. Chem. 1994; 98:1978.
45. Nicholls A, Honig B. Journal of Computational Chemistry. 1991; 12:435.
46. Sharp KA, Honig B. Annual Review of Biophysics and Biophysical Chemistry. 1990; 19:301.
47. Jean-Charles A, Nicholls A, Sharp K, Honig B, Tempczyk A, Hendrickson TF, Still WC. Journal of the American Chemical Society. 1991; 113:1454.
48. Gilson MK, Honig B. Journal of Computer-Aided Molecular Design. 1991; 5:5. [PubMed: 2072125]
49. Schiffer CA, Caldwell JW, Stroud RM, Kollman PA. Protein Science. 1992; 1:396. [PubMed: 1304346]
50. Smith KC, Honig B. Proteins: Structure, Function, and Genetics. 1994; 18:119.
51. Zauhar RJ. Journal of Computational Chemistry. 1991; 12:575.
52. Ulmschneider JP, Jorgensen WL. Journal of the American Chemical Society. 2004; 126:1849. [PubMed: 14871118]
53. Tannor DJ, Marten B, Murphy R, Friesner RA, Sitkoff D, Nicholls A, Honig B, Ringnalda M, Goddard WA. Journal of the American Chemical Society. 1994; 116:11875.
54. Fraser RR, Boussard G, Saunders JK, Lambert JB, Mixan CE. J. Am. Chem. Soc. 1971; 93:3822.
55. Momany FA, McGuire RF, Burgess AW, Scheraga HA. J. Phys. Chem. 1975; 79:2361.
56. Altenbach C, Oh K, Trabanino RJ, Hideg K, Hubbell WL. Biochemistry. 2001; 40:15471. [PubMed: 11747422]
57. Altenbach C, Kusnetzow AK, Ernst OP, Hofmann KP, Hubbell WL. Proceedings of the National Academy of Sciences. 2008; 105:7439.
58. Bhattacharyya R, Pal D, Chakrabarti P. Protein Engineering, Design and Selection. 2004; 17:795.
59. Bleiholder C, Gleiter R, Werz DB, Koppel H. Inorg. Chem. 2007; 46:2249. [PubMed: 17311376]
60. Iwaoka M, Takemoto S, Okada M, Tomoda S. Chemistry Letters. 2001; 30:132.
61. Iwaoka M, Takemoto S, Okada M, Tomoda S. Bulletin of the Chemical Society of Japan. 2002; 75:1611.
62. Pal D, Chakrabarti P. Journal of Biomolecular Structure and Dynamics. 2001; 19:115. [PubMed: 11565843]
63. Glusker JP. Top. Curr. Chem. 1998; 198:1.
64. Rosenfield RE, Parthasarathy R, Dunitz JD. Journal of the American Chemical Society. 1977; 99:4860.
65. Bondi A. J. Phys. Chem. 1964; 68:441.
66. Van Wart HE, Scheraga HA. Proceedings of the National Academy of Sciences of the United States of America. 1977; 74:13. [PubMed: 264666]
67. Weiss MS, Brandl M, Sühnel J, Pal D, Hilgenfeld R. Trends in Biochemical Sciences. 2001; 26:521. [PubMed: 11551776]
68. Van Wart HE, Shipman LL, Scheraga HA. The Journal of Physical Chemistry. 1975; 79:1428.
69. Spencer JN, Casey GJ Jr, Buckfelder J, Schreiber HD. The Journal of Physical Chemistry. 1974; 78:1415.

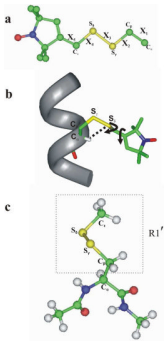

Figure 1.

(a) The R1 side chain with definition of the dihedral angles and atom designation. (b) The R1 side chain at a solvent exposed site in a α-helix. The dashed lines indicate the interaction of S_δ with $C_\alpha H$ group which inhibits rotations about X_1–X_3. The arrows indicate the allowed motion about X_4 and X_5 that most influence the EPR spectra of R1. (c) R1 side chain fragment (R1′) used in calculations in a single residue model peptide. The N-terminus and C-terminus of the peptide are capped by acetyl and N-methyl groups respectively.

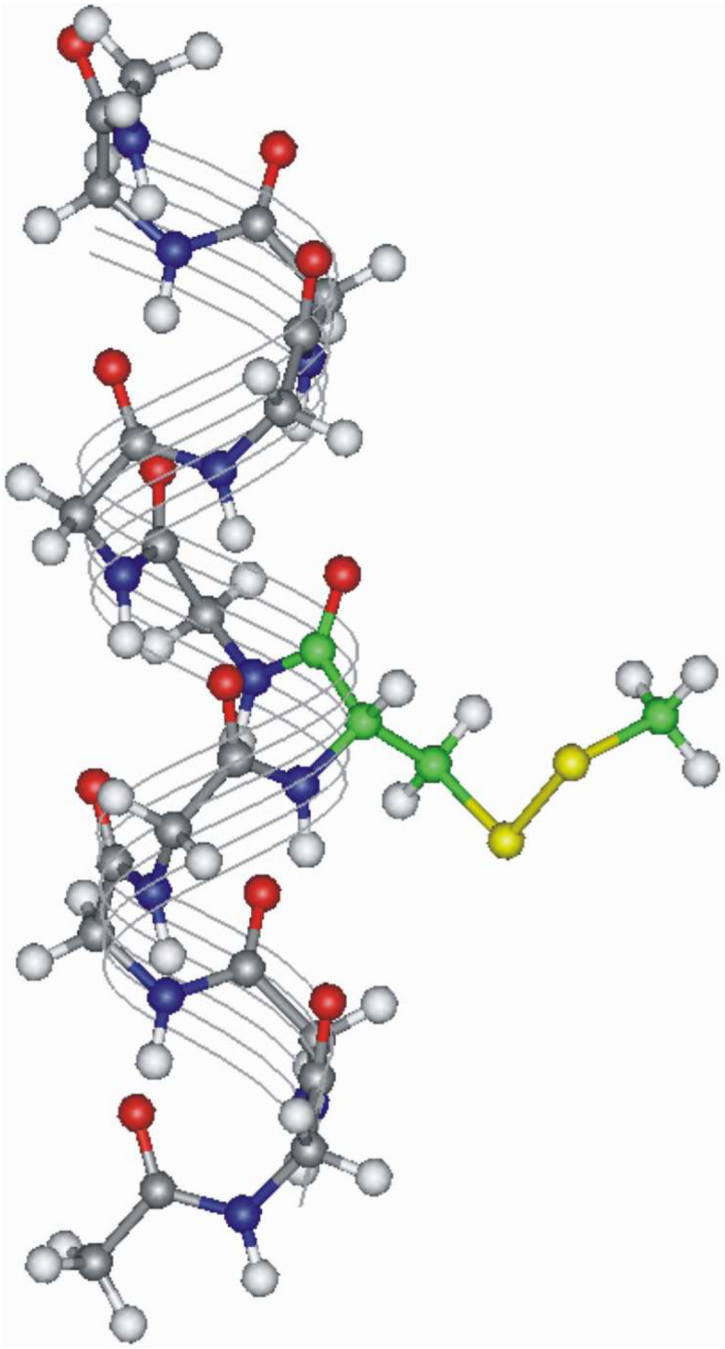

Figure 2.
R1′ in a ten residue α-helix. The N-terminus and C-terminus of the helix are capped by acetyl and N-methyl groups respectively.

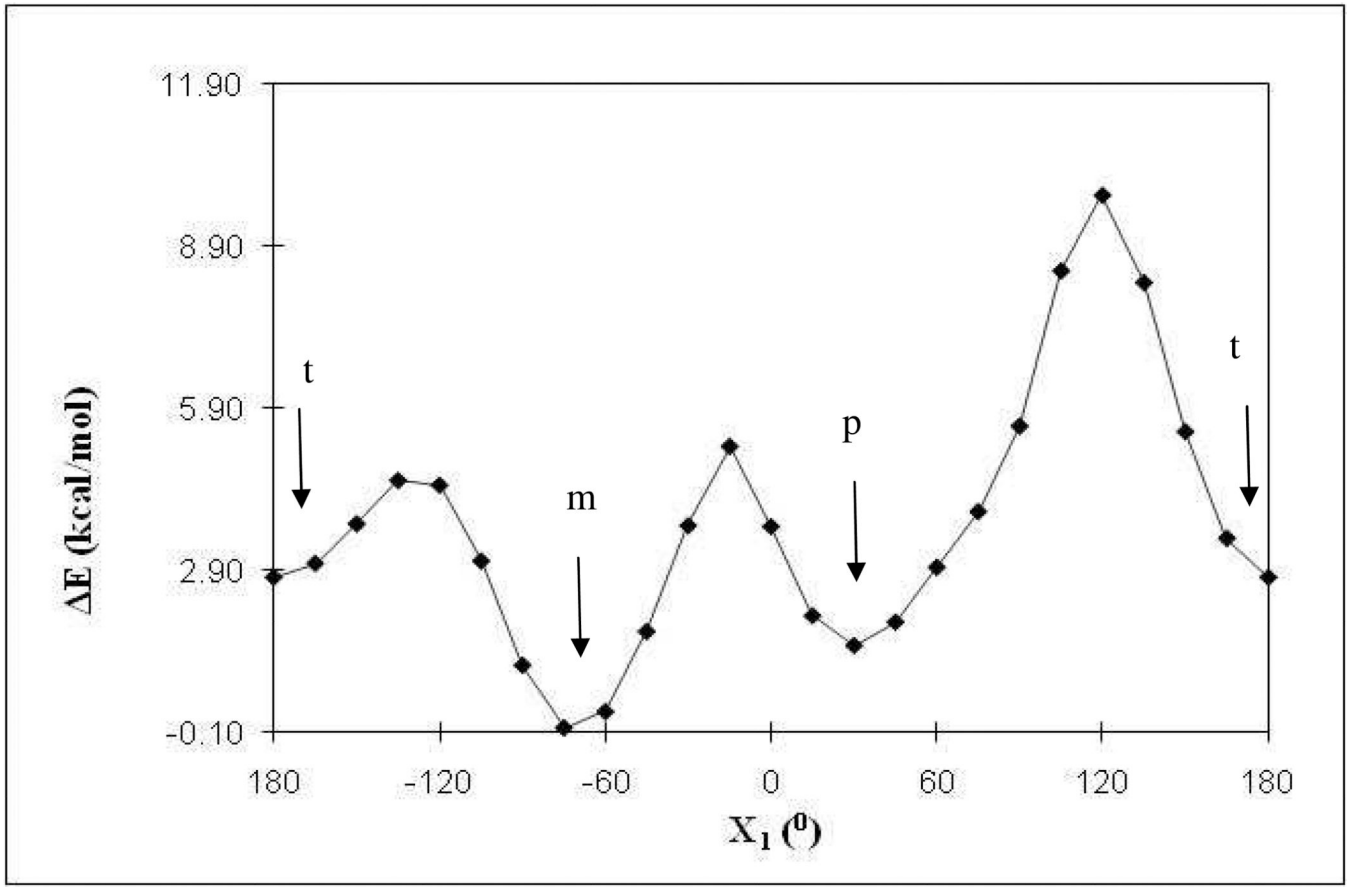

Figure 3.
Relaxed scan for X_1 when X_2=60 and X_3=90. The arrows identify the energy minima corresponding to the indicated rotamer (see text for definition). Energies are B3LYP/6-31G(d) electronic energies, relative to the energy of the lowest energy minimum.

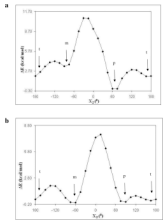

Figure 4.
Relaxed scan for X_2 when (a) X_1=180 and X_3=−90, and(b) X_1=−60 and X_3=90. The arrows identify the energy minima corresponding to the indicated rotamer (see text for definition). Energies are B3LYP/6-31G(d) electronic energies, relative to the energy of the lowest energy minimum.

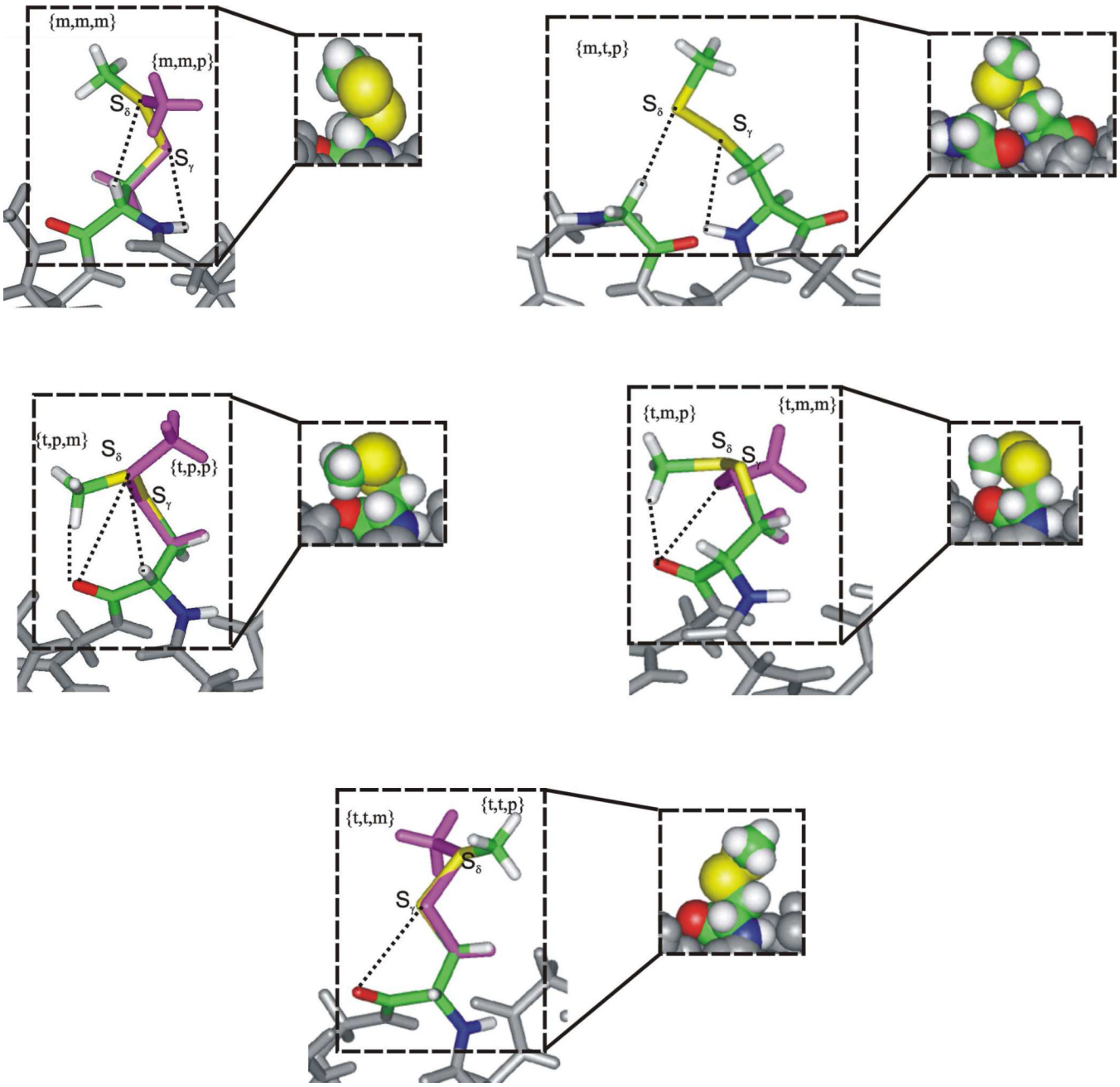

Figure 5.

Optimized conformations of the R1′. Carbon (green), sulfur (yellow), nitrogen (blue) and oxygen (red) atoms are highlighted for the lowest energy conformations of R1′ about X_3 angle and for residues that interact with it. The higher energy conformer of R1′about X_3 angle is shown in purple. The insets are CPK representations that show van der Waals contact between interacting atoms.

TABLE 1

Rotamers of R1 and corresponding interatomic distances from crystal structures

PDB ID	mutant	rotamer	temperature (K)	X_1 (°)	X_2 (°)	X_3 (°)	d(N···S_γ) (Å)	d(C=O···S_γ) (Å)	d(C=O···S_δ) (Å)	d(C_α-H···S_δ) (Å)
2Q9E[a]	44R1 (chain A)	{m,m}	100	−83	−58	−95	3.35	4.65	4.59	2.66
2Q9E[a]	44R1 (chain B)	{m,m}	100	−85	−55	−96	3.38	4.70	4.54	2.60
1ZYT[b]	82R1	{m,m}	100	−68	−56	101	3.14	4.56	4.77	2.65
2IGC[c]	115R1	{m,m}	100	−81	−57	−92	3.53	4.75	4.85	3.07
2OU8[c]	115R1	{m,m}	298	−94	−28		3.69	4.63	4.75	2.80
2CUU[b]	131R1 (conformation 1)	{m,m}	100	−69	−60		3.12	4.74	4.87	2.69
3G3V[b]	131R1 (conformation 1)	{m,m}	291	−75	−57		3.24	4.69	4.89	2.81
3G3X[b]	151R1	{m,m}	100	−83	−72		3.30	4.56	4.54	2.88
3G3W[b]	151R1	{m,m}	291	−82	−72		3.28	4.57	4.60	2.85
Average		{m,m}		−80	−57		3.34	4.65	4.71	2.78
2Q9D[a]	41R1	{t,p}	100	−175	57	86	4.17	3.42	3.86	3.12
2CUU[b]	131R1 (conformation 2)	{t,p}	100	175	80		4.06	3.33	4.19	3.29
3G3V[b]	131R1 (conformation 2)	{t,p}	291	175	83		4.02	3.20	4.16	3.26
Average		{t,p}		175	73		4.08	3.32	4.07	3.22
2Q9E[a]	44R1 (chain C)	{t,m}	100	173	−96		4.06	3.29	3.73	4.48
2OU8[c]	115R1	{t,m}	298	163	−63		4.16	3.46	3.33	4.25
Average		{t,m}		168	−80		4.11	3.38	3.53	4.37

[a] Guo *et al.*[12],

[b] Fleissner *et al.*[19],

[c] Guo *et al.*[13]

TABLE 2

Dihedral angles, intra-residue distances between S and backbone atoms[a] and relative gas phase conformational energies for the optimized rotamers of R1′ in a 10 residue α-helix

	X_1	X_2	X_3	$d(N\cdots S_\gamma)$	$d(C{=}O\cdots S_\gamma)$	$d(C{=}O\cdots S_\delta)$	$d(C_\alpha\text{-}H\cdots S_\delta)$	$\Delta(E+D)_{conf}$ (kcal/mol)[b]
tpm	−180	64	−101	4.14	3.58	4.12	3.11	0.00
mmm	−67	−64	−83	3.32	4.87	5.03	3.01	0.58
mtp	−71	153	85	3.26	4.80	6.34	4.83	0.69
mmp	−64	−71	95	3.30	4.91	5.15	3.17	0.79
tmp	−160	−91	103	4.12	3.82	3.82	4.29	1.48
tpp	−180	63	89	4.13	3.51	4.00	3.04	4.19
tmm	−171	−85	−91	4.12	3.59	3.47	4.23	4.21
ttp	−174	178	90	4.09	3.41	5.39	4.75	4.45
ttm	−178	170	−90	4.10	3.35	5.41	4.71	4.83

[a] sum of van der Waals radii for specific pairs: $r_{vdW}(N\cdots S)$=3.35 Å, $r_{vdW}(S\cdots O)$=3.32Å, $r_{vdW}(H\cdots S)$=3.00 Å.[65]

[b] given relative to the lowest energy conformation; calculated with B3LYP/6–31G(d)+D electronic energies.

TABLE 3

Gas phase, solvation and total energies for R1' rotamers in a 10 turn helix Conformational energies are calculated using the dispersion corrected functional B3LYP-D

rotamer[a]	$\Delta(E+D)_{conf}$ (kcal/mol)[b]	ΔG_{ele} (kcal/mol)[b]	ΔG_{np} (kcal/mol)[b]	ΔG_{total} (kcal/mol)[b]
tpm	0.00	3.26	0.22	0.00
mmp	0.79	3.22	0.57	1.11
tmp	1.48	3.77	0.00	1.77
mmm	0.58	3.77	1.05	1.91
tmm	4.21	0.52	0.72	1.96
tpp	4.19	0.00	1.32	2.03
mtp	0.69	4.69	0.57	2.47
ttp	4.45	0.77	1.30	3.03
ttm	4.83	0.41	1.62	3.38

[a] The order of rotamers is increasing energy.

[b] In each column, the energy is given relative to the lowest state.